Radiofrequency ablation in combination with an mTOR inhibitor restrains pancreatic cancer growth induced by intrinsic HSP70

Shanshan Gao*, Ning Pu*, Hanlin Yin, Junhao Li, Qiangda Chen, Minjie Yang, Wenhui Lou, Yi Chen, Guofeng Zhou, Changyu Li, Guoping Li, Zhiping Yan, Lingxiao Liu, Jun Yu and Xiaolin Wang

Ther Adv Med Oncol

2020, Vol. 12: 1–15

DOI: 10.1177/1758835920953728

Abstract

Background: Radiofrequency ablation (RFA) is widely used in palliative therapy of malignant cancers. Several studies have shown its applicability and safety for locally advanced pancreatic cancer (LAPC). The objective of this study was to modify the current regimen to improve its therapeutic effect.

Methods: Immune cell subtypes and related cytokines were quantified to uncover the immune pattern changes post-RFA treatment. Then, high-throughput proteome analysis was performed to identify differentially expressed proteins associated with RFA, which were further validated in *in vitro* and *in vivo* experiments. Finally, a combined therapy was tested in a murine model to observe its therapeutic effect.

Results: In preclinical murine models of RFA treatment, no significant therapeutic benefit was observed following RFA treatment. However, the proportion of tumor-infiltrating $CD8^+$ T cells was significantly increased, whereas that of regulatory T cells (Tregs) was decreased post-RFA treatment, which indicated a beneficial anti-tumor environment. To identify the mechanism, high-throughput mass spectrum was obtained that identified heat shock protein 70 (HSP70) as the top differentially expressed protein. HSP70 expression in residual cancer cells was significantly increased post-RFA treatment, which notably promoted pancreatic cancer growth. Elevated HSP70 promoted cell proliferation by activating AKT–mTOR signaling. Finally, RFA treatment combined with an mTOR inhibitor exerted a synergetic repressive effect on tumor growth in the preclinical murine cancer model.

Conclusions: RFA treatment in combination with mTOR signaling blockade can not only promote tumor immune response, but also restrain residual cancer cell proliferation. Such a combination may be a promising and effective therapeutic strategy for LAPC patients.

Keywords: heat shock protein 70, mammalian target of rapamycin, microenvironment, pancreatic ductal adenocarcinoma, radiofrequency ablation

Received: 21 April 2020; revised manuscript accepted: 6 August 2020.

Correspondence to:
Xiaolin Wang
Lingxiao Liu
Department of Interventional Radiology, Zhongshan Hospital, Fudan University, 180 Fenglin Road, Shanghai 200032, China
Shanghai Institute of Medical Imaging, Fudan University, Shanghai, China
wang.xiaolin@zs-hospital.sh.cn
liu.lingxiao@zs-hospital.sh.cn

Jun Yu
Department of Surgery, The Sol Goldman Pancreatic Cancer Research Center, The Johns Hopkins University School of Medicine, 600 N. Wolfe Street, Baltimore, MD 21287, USA
jyu41@jhmi.edu

Shanshan Gao
Department of Interventional Radiology, Zhongshan Hospital, Fudan University, Shanghai, China
Shanghai Institute of Medical Imaging, Fudan University, Shanghai, China
Department of Surgery, The Sol Goldman Pancreatic Cancer Research Center, The Johns Hopkins University School of Medicine, Baltimore, MD, USA

Ning Pu
Department of General Surgery, Zhongshan Hospital, Fudan University, Shanghai, China
Department of Surgery, The Sol Goldman Pancreatic Cancer Research Center, The Johns Hopkins University School of Medicine, Baltimore, MD, USA

Hanlin Yin
Qiangda Chen
Wenhui Lou
Department of General Surgery, Zhongshan

Introduction

Pancreatic ductal adenocarcinoma (PDAC) is one of the most malignant cancers in the digestive tract. Its mortality is extremely high, and the 5-year cumulative survival rate remains less than 9%, and has barely improved over the past few decades.[1] At present, radical resection is still the only potentially curative strategy for PDAC, but only 15–20% of patients have the chance of surgery when diagnosed, and most of them lose the opportunity due to locally advanced disease.[2] Interventional chemotherapy is the most common palliative intervention modality for locally advanced pancreatic cancer (LAPC), which directly delivers chemotherapy drugs into the tumor through tumor-surrounding arteries. The advantages of this treatment include increased topical concentration and reduced systemic toxicity compared to systemic

Hospital, Fudan University, Shanghai, China

Junhao Li
Minjie Yang
Yi Chen
Changyu Li
Guoping Li
Zhiping Yan
Department of Interventional Radiology, Zhongshan Hospital, Fudan University, Shanghai, China

Shanghai Institute of Medical Imaging, Fudan University, Shanghai, China

Guofeng Zhou
Shanghai Institute of Medical Imaging, Fudan University, Shanghai, China

Department of Radiology, Zhongshan Hospital, Fudan University, Shanghai, China

*These authors contributed equally

chemotherapy.[3] Even though interventional chemotherapy has achieved certain efficacy, the benefit in overall survival (OS) is still limited due to the poor sensitivity to chemotherapy.[4] Another reason resulting in poor prognosis is the immunosuppressive microenvironment, which contains regulatory T cells (Tregs), impairs cytotoxic T lymphocytes (CTLs), and promotes tumor immune escape.[5] Therefore, it is imperative to explore novel and effective therapeutic strategies to improve the prognosis of LAPC.

Radiofrequency ablation (RFA) is a minimally invasive procedure widely used in unresectable or metastatic solid cancers, which can cause coagulative necrosis in the center of tumors through high-frequency alternating current.[6] So far, most studies on RFA have focused on hepatocellular carcinoma (HCC), which showed RFA could not only effectively kill HCC cells but also stimulate a specific antitumor immune response.[7,8] Moreover, during RFA treatment of multiple HCC, researchers found that tumor lesions that were not exposed to RFA had subsided spontaneously as well, which further supported the function of RFA as a potential immunomodulatory therapy.[9] However, the efficacy of RFA treatment for LAPC is still controversial.

The limited use of RFA in LAPC is partly due to the high sensitivity of normal pancreatic tissue to heat and to the close anatomical position to vessels and bile ducts, which may lead to a high risk of complications when applying this technology. Recently, with thinner RFA probes in combination with the application of real-time dynamic ultrasound guidance and monitoring systems, the morbidity and mortality of postoperative complications have significantly declined.[10] An increasing number of studies has shown that RFA treatment of LAPC patients is a safe and potential palliative therapy.[10–12] However, no obvious clinical benefits have been achieved from RFA treatment of LAPC patients.[13,14] Furthermore, a more aggressive phenotype of residual cancer cells and poor prognosis have even been observed in HCC after RFA treatment.[15,16] However, no study has revealed the reasons for the limited benefits of RFA treatment in LAPC, and the underlying mechanism involving the microenvironment and the biological behaviors of residual cancer cells after RFA treatment is still unknown.

Here, we report that RFA treatment alone in orthotopic murine models can promote tumor immune response but it concomitantly increases heat shock protein 70 (HSP70) expression in residual cancer cells, which promotes residual cancer cell proliferation. The major underlying mechanism involves HSP70-mediated activation of the AKT-mammalian target of rapamycin (mTOR) signaling to promote tumor progression. More importantly, RFA treatment in combination with mTOR inhibitors results in synergistic and durable tumor suppression compared to either regimen used alone.

Materials and methods

Murine and human cell lines

The murine pancreatic cancer cell line Panc02 was a gift from the Department of Pancreatic Surgery, Zhongshan Hospital. Human pancreatic cancer cell lines BxPC-3, MIA-PaCa-2, PANC-1, and SW1990, and the normal pancreatic ductal cell line HPDE were obtained from the Chinese Academy of Sciences. Panc02, BxPC-3, and SW1990 were cultured in RPMI-1640 medium (Gibco, Carlsbad, CA, USA), while MIA-PaCa-2 and PANC-1 were cultured in high-glucose Dulbecco's Modified Eagle's Medium (Gibco). All culture media were supplemented with 10% fetal bovine serum (Gibco) and 1% penicillin/streptomycin (Gibco), and cell cultures were maintained on a 5% carbon dioxide (CO_2) humidified atmosphere at 37°C. In addition, the culture medium of MIA-PaCa-2 cells was supplemented with 2.5% horse serum.

To examine the effect of mTOR or AKT inhibitors, the culture medium of cells was supplemented with 0.5 μM mTOR inhibitors or 1.0 μM AKT inhibitors, while dimethylsulfoxide (DMSO) solution was added as control.

Orthotopic and subcutaneous murine tumor models

Six-week-old C57BL/6 mice and 5-week-old BALB/c nude mice (Jiesijie Laboratory Animals Co. Ltd., Shanghai, China) were maintained in a specific pathogen-free (SPF) environment, and all procedures complied with the China Animal Welfare Guidelines. A total of 30 C57BL/6 mice were orthotopically inoculated with 2×10^6 Panc02 cells/inoculum and divided into two cohorts with three time points (days 1, 3 and 7). Their tumor volumes were assessed by 3.0-tesla magnetic resonance imaging (MRI) scanning: T1

weighted imaging (T1WI) and T2 weighted imaging (T2WI) based on our previous publication and RFA was performed when the tumor volume was nearly 1 cm^3.[17] Twenty BALB/c nude mice were subcutaneously inoculated with 1×10^7 transfected cells/inoculum to evaluate the HSP70 function in two different cell lines. The protocols for this study were approved by the Research Ethics, Institutional Animal Care and Use Committee of Zhongshan Hospital, Fudan University (no. 2018-131). The tumor length and width were recorded, and the tumor volume was estimated by (length $\times$ width^2)/2. Finally, 16 C57BL/6 mice were subcutaneously inoculated with 2×10^6 Panc02 cells/inoculum and divided into four groups with different treatments. RFA was performed when tumor volume was nearly 1 cm^3, and 1.5 mg/kg INK-128 was administered orally 1 h before RFA and again 6 h after RFA, followed by two additional doses separated by 7 h, starting the next day and for 2 weeks.

Operation of radiofrequency ablation and its mimics in vitro

A small incision was made along the left costal arch of the abdomen to expose the orthotopic tumor of the pancreas. The RFA probe (EMcision Ltd., London, UK) was guided by a 21-gauge puncture needle into the tumor that was treated at 5 Watts for 90 s. Under the same conditions, an RFA needle was inserted in the control group, but no RFA treatment was performed. In mimics, pancreatic cancer cells were seeded into 6-well plates (5×10^4 cells/well) and further incubated for another 24 h. Then, culture medium was replaced with 1 mL of fresh medium, and plates were sealed and incubated in a water bath with the temperature gradually increasing from 37°C to 50°C within 10 min. After thermal treatment, 1.5 mL fresh medium was further added to the cells in each well and then maintained in the incubator. In the control group, cells were incubated in a water bath at 37°C for 10 min.

Flow cytometry and antibodies

Murine red blood cells in peripheral blood and spleens were lysed with lysing buffer (BD Bioscience, Franklin Lakes, NJ, USA) and tumor tissues were digested with collagenase IV (Gibco) for single-cell suspensions. The cell pellets were filtrated through 70 μm strainers and then stained with FITC-CD3 (BD Bioscience), PerCP-Cy5.5-CD4 (BD Bioscience), PE-Cy7-CD8 (BD Bioscience) and Alex Fluorescence 647-FoxP3 (BD Bioscience) for detecting the populations of $CD4^+$, $CD8^+$ and $CD4^+$ $FoxP3^+$ Tregs among $CD3^+$ T lymphocytes. Annexin V: FITC Apoptosis Detection Kit and Annexin V Alexa Fluor 647 conjugate (BD Bioscience) were used to detect cell apoptosis. All experiments were performed in a FACS Aria II flow cytometer (BD Bioscience).

Immunohistochemistry

Formalin-fixed, paraffin-embedded (FFPE) tumor specimens were stained with hematoxylin-eosin to observe their histomorphology. Rabbit anti-CD8 (Abcam, Cambridge, UK), Rabbit anti-Ki-67 (Abcam) and Rabbit anti-HSP70 (Cell Signaling Technology, Danvers, MA, USA) monoclonal antibodies were used for immunohistochemistry (IHC) staining as described previously.[18] The number of $CD8^+$ infiltrating lymphocytes were measured in three independent 400$\times$ high-power fields (HPFs) by two individuals blinded to the specimens.

Enzyme-linked immunosorbent assay

Tumor tissue homogenates were prepared with radio-immunopreciptation assay (RIPA) lysis buffer containing 1% phenylmethanesulfonyl fluoride (PMSF). According to the manufacturer's instructions and our previous publication, the concentrations of transforming growth factor β (TGF-β) and interferon γ (IFN-γ) were determined by enzyme-linked immunosorbent assay (ELISA) kit (R&D Systems, Tustin, CA, USA) as our previous publication.[19]

High-throughput proteomic analysis

The Triple TOF 4600 mass spectrometer was used to detect and analyze the protein spectra. The mass spectrometry was performed on the public sharing platform of the Institutes of Biomedical Sciences (IBS) of Fudan University under the guidance of professional technologists. Differentially expressed proteins were identified through fold-change filtering.

Lentivirus construction and transfection

MIA-PaCa-2 wild-type cells were transfected by the lentiviral vector containing Ubi-HSP70-3FLAG-SV40-EGFP-IRES-puromycin, whereas PANC-1 wild-type cells were transfected by the lentiviral vector containing hU6-HSP70-ubiquitin-EGFP-IRES-puromycin.

5′-GAGGATCCCCGGGTACCGGTCGCCACCATGGCCAAAGCCGCGGCGATCGG-3′ (forward) and 5′-TCCTTGTAGTCCATACCATCTACCTCCTCAATGGTGGGGCC-3′ (reverse) were the sequences for the primers used for the human HSP70 gene, and 5′-CTGTTTGTCAGTTCTCAATTT-3′ was the target logical sequence for human HSP70 shRNA. In addition, the lentiviral vectors containing Ubi-3FLAG-SV40-EGFP-IRES-puromycin or hU6-control-ubiquitin-EGFP-IRES-puromycin were used as controls.

RNA isolation, reverse transcription and quantitative real-time polymerase chain reaction (qRT-PCR)

Total RNAs were isolated from HPDE, BxPC-3, MIA-PaCa-2, PANC-1, and SW1990 cells. PrimeScript reverse transcriptase Master Mix (Takara Bio Inc., Otsu, Shiga, Japan) and SYBR Premix Ex Taq (Takara Bio Inc.) were used as previously reported.[18] The specific primers were designed for detecting human GAPDH (forward: 5′-GGAGCGAGATCCCTCCAAAAT-3′, reverse: 5′-GGCTGTTGTCATACTTCTCATGG-3′) and HSP70 (forward: 5′-GCAGAACACCGTGTTTGACGC-3′, reverse: 5′-CCTGGAAAGGCCAGTGCTTCA-3′).

Western immunoblots and antibodies

Total proteins were quantified by BCA Protein Assay Kit (Beyotime, Shanghai, China) and separated in 10% sodium dodecyl sulfate-polyacrylamide gel electrophoresis (SDS-PAGE) (Beyotime), and then electro-transferred onto polyvinylidene fluoride (PVDF) membranes (Millipore, Billerica, MA, USA). After 1 h block in 5% non-fat milk, the PVDF membranes were incubated with primary antibodies and secondary antibody, and detected with Tanon 5200 Image System (Tanon, Shanghai, China) according to our previously published protocols.[18] The primary antibodies used are listed in Supplemental Table 1.

Proliferation and colony formation

For proliferation assay, 1000 pancreatic cancer cells per well were seeded in 96-well plates and observed for 96 h. According to the manufacturer's instructions, the optical density (OD) values at 450 nm at 0, 24, 48, 72, 96 h were detected by the microplate reader (Bio-Rad, Hercules, CA, USA) after it was mixed with Cell-Counting Kit (Dojindo Molecular Technologies, Shanghai, China) for an additional 2 h incubation to reveal tumor cell count.

For colony formation assay, 500–1000 cells per well were seeded in 6-well plates and cultured for 2 weeks. Then, 1% paraformaldehyde was used to fix cells for 30 min and the cells were stained with crystal violet solution for 30 min. The number of cell colonies was calculated by Image-Pro Plus 5.0 software (Media Cybernetics, Bethesda, MD, USA). All experiments were independently repeated three times in triplicate.

Statistical analyses

The statistical software of SPSS v21.0 (IBM Corporation, Armonk, NY, USA) was used for statistical analysis. The data of the experiments are expressed as mean ± standard deviation. The comparisons of quantitative data with normal distribution were assessed by two-tailed Student's *t*-tests or one-way analysis of variance (ANOVA) with additional least-significant difference (LSD) or Tamhane methods. Graphs for experimental data were prepared using GraphPad Prism 6.0 software (GraphPad Software, La Jolla, CA, USA) and ImageJ software (National Institutes of Health, Bethesda, MD, USA) was used to determine the density of the western blot bands. The p value of <0.05 was considered statistically significant.

Results

Limited benefits derived from RFA alone in orthotopic PDAC murine models

To measure the efficacy of RFA treatment alone in PDAC murine models, Panc02 cells were cultured and injected into the pancreas to establish the orthotopic PDAC models in immunocompetent C57BL/6 mice (Figure 1A). Then, they were followed up with magnetic resonance imaging (MRI) scanning until the maximum diameter of the tumors reached about 1 cm, which resembled a spherical growth pattern and displayed a mixed signal on T2-weighted images in the transverse plane (Figure 1B).

After RFA treatment, the median tumor volumes in the RFA cohort were $742.00 \pm 163.72\,mm^2$, $1067.70 \pm 231.58\,mm^2$ and $1319.9 \pm 300.59\,mm^2$ on days 1, 3 and 7, respectively, while those of the control cohort were $713.80 \pm 181.76\,mm^2$, $1099.6 \pm 219.56\,mm^2$ and $1385 \pm 177.86\,mm^2$, respectively. However, no statistically significant

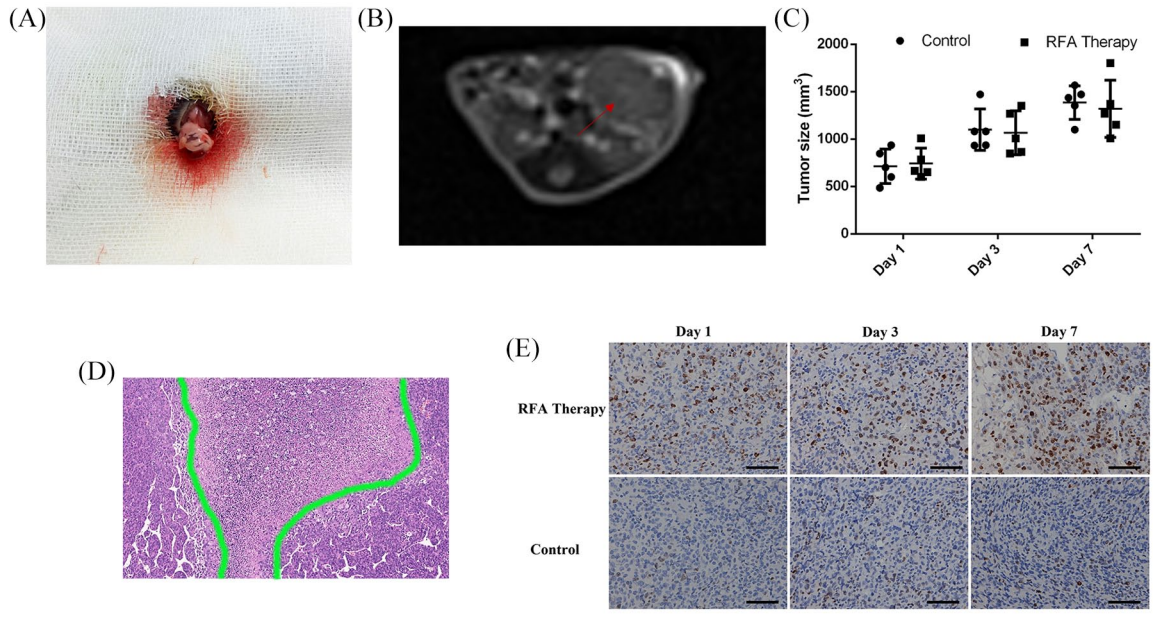

Figure 1. The orthotopic PDAC murine models for RFA treatment. (A) Cell inoculation into the pancreas under surgery. (B) Follow-ups with MRI scanning in transverse plane; the tumor is marked with a red arrow. (C) Comparison of tumor volumes with or without RFA therapy on days 1, 3 and 7. (D) The typical necrotic area in the center of tumor post-RFA treatment. (E) Ki-67 staining of the residual tumor tissues with or without RFA therapy. MRI, magnetic resonance imaging; PDAC, pancreatic ductal adenocarcinoma; RFA, radiofrequency ablation.

difference was observed between these two cohorts (Figure 1C), which may be the result of the short observational interval or of changes in tumor biological characteristics. Pathological examination of the tumor tissues after RFA treatment indicated a necrotic area in the center of the tumor tissue (Figure 1D). Then, the Ki-67 staining of the residual tumor tissues gradually increased in intensity and area over time after RFA treatment and was obviously higher than that in the control cohort (Figure 1E), which indicated that RFA may potentially promote residual cancer cell proliferation resulting in limited benefits from RFA treatment.

RFA treatment enhanced the immune response in the tumor microenvironment

Previous reports have proposed that the immune patterns in the tumor microenvironment may also be influenced by thermal ablation.[6] Thus, the changes in the immune landscape after RFA treatment were examined in tumor tissues. The proportions of $CD3^+CD4^+$ T cells, $CD3^+CD8^+$ T cells, and $CD4^+FoxP3^+$Treg cells in the spleen, blood and tumor are shown in Supplemental Table 2. The results from flow cytometry showed that there was no significant difference in $CD4^+$ T and $CD8^+$ T cell distribution in the spleens and peripheral blood mononuclear cells (PBMCs) between the RFA treatment cohort and the control cohort (Supplemental Figure 1A–E). Intriguingly, a transient decline was observed in the proportion of $CD4^+$ T cells after RFA treatment on day 3 (Supplemental Figure 1D), which may result from the trauma stress-induced temporary immune suppression. In the tumor microenvironment, no difference in the proportion of infiltrating $CD4^+$ T cells was observed as well (Supplemental Figure 1F). However, as a small proportion of infiltrating $CD8^+$ T cells existed in tumor tissues, we further applied the IHC staining to determine infiltrating $CD8^+$ T cells. IHC staining showed that the proportion of infiltrating $CD8^+$ T cells was significantly increased after RFA treatment on days 1, 3, and 7 (Figure 2E and F). Treg cells play a vital role in PDAC progression and inhibit immune response in the tumor microenvironment.[19] Thus, we further examined the presence of $CD4^+FoxP3^+$Treg cells in the spleen, blood, and tumor (Figure 2A). The results showed that there was no difference in the proportion of Treg cells in the spleens after RFA treatment (Figure 2B), but in the blood and tumor microenvironment, the proportions of Treg cells were significantly decreased on days 1, 3 and 7 (Figure 2C and D), which indicated an impairment in immune suppression.

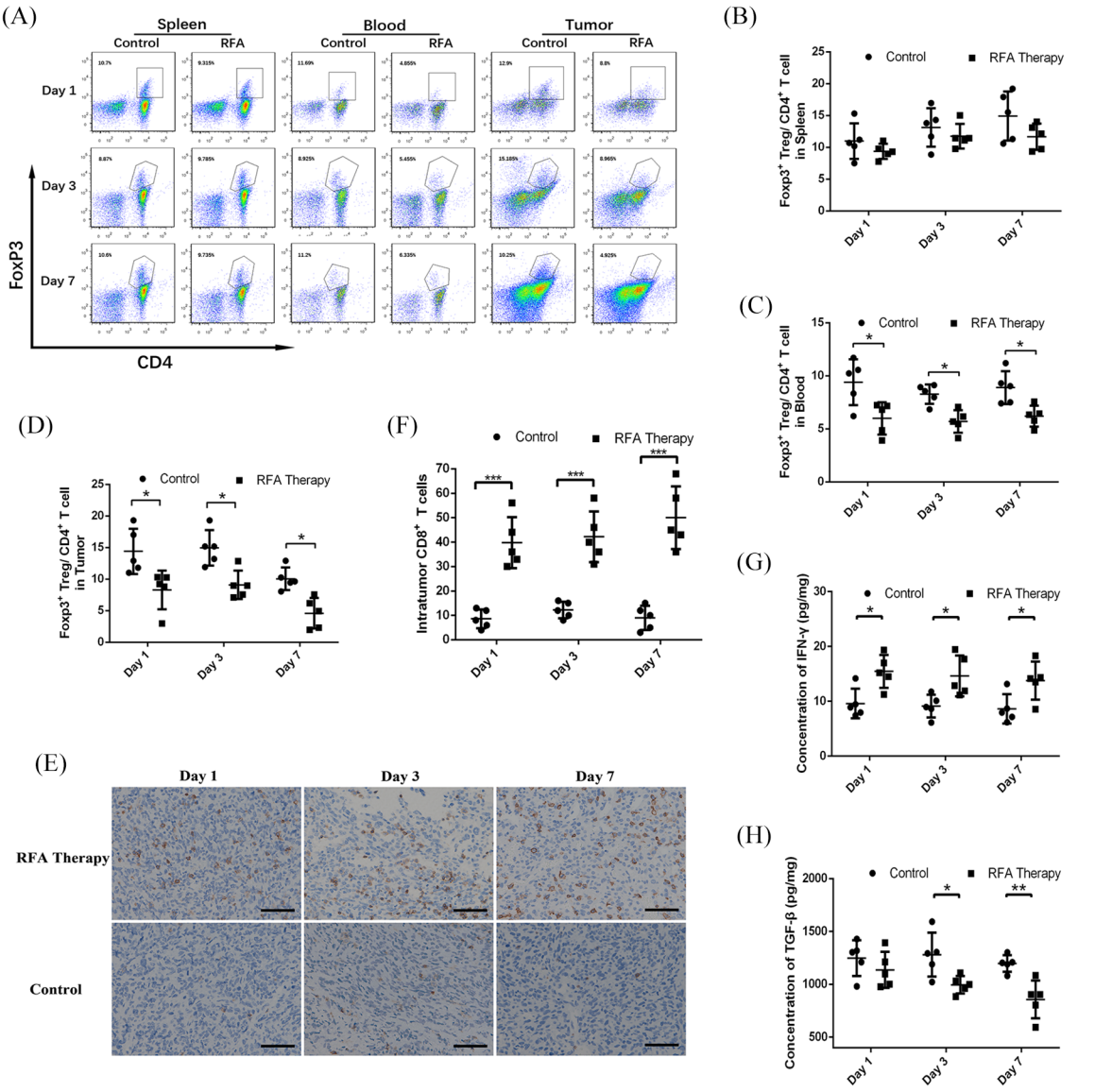

Figure 2. The changes of immune patterns in murine PDAC models after RFA treatment. (A) Flow cytometry data and statistical diagrams showing the proportions of $CD4^+FoxP3^+$ Tregs in the (B) spleens, (C) blood and (D) tumor tissues with or without RFA treatment on days 1, 3, and 7. (E) Representative immunohistochemistry staining and (F) statistical diagram showing the proportion of infiltrating $CD8^+$ T cells in the residual tumor tissues. The concentrations of (G) IFN-γ and (H) TGF-β in the tumor tissues.
IFN-γ, interferon gamma; PDAC, pancreatic ductal adenocarcinoma; RFA, radiofrequency ablation; TGF-β, transforming growth factor beta; Tregs, regulatory T cells.
*p-value < 0.05, **p-value < 0.01, ***p-value < 0.001.

In addition, IFN-γ is widely considered a marker of tumor immune response. ELISA was used to detect changes in its level in the tumor microenvironment. The results showed that the concentrations of IFN-γ were significantly increased in tumor tissue homogenates 1, 3 and 7 days post-RFA treatment (Figure 2G). Then, considering the role of TGF-β in Treg differentiation or secretion, mesenchyme formation, and tumor promotion, its concentration in tumor tissue homogenates was analyzed. A significant decline in the levels of TGF-β post-RFA treatment was observed on days 3 and 7 but not on day 1, which may be due to a delayed response (Figure 2H). The concentrations of IFN-γ and TGF-β are listed in Supplemental Table 3. Therefore, RFA treatment could create an immune advantage and promote tumor immune

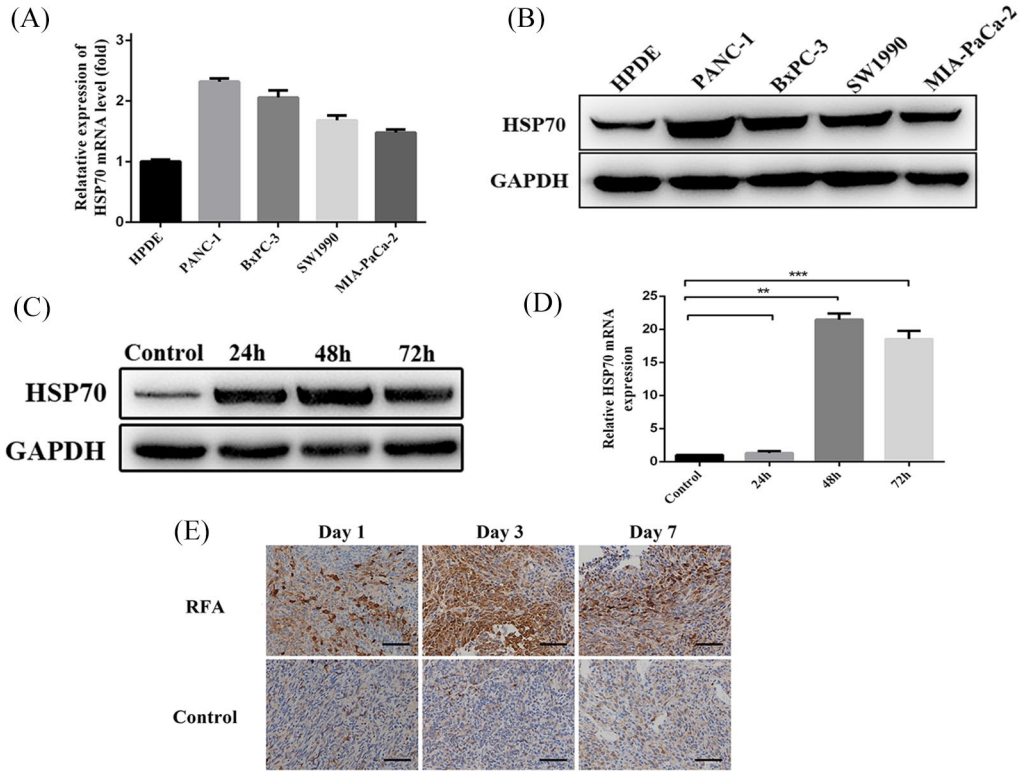

Figure 3. HSP70 expression in cell lines and residual tumor tissues. HSP70 expression detected by (A) qRT-PCR and (B) western blot in four PDAC cell lines and normal HPDE cells. (C) Western blot and (D) qRT-PCR analysis for HSP70 expression after *in vitro* stimulation of MIA-PaCa-2 cells. (E) Representative immunohistochemistry staining of HSP70 in residual tumor tissues from orthotopic PDAC murine models days 1, 3 and 7 post-RFA treatment.
HSP70, heat shock protein 70; PDAC, pancreatic ductal adenocarcinoma; RFA, radiofrequency ablation; qRT-PCR, quantitative real-time polymerase chain reaction.
$^{**}p$-value < 0.01, $^{***}p$-value < 0.001.

response. However, limited benefits from RFA alone may be mainly caused by disruption of tumor biological behaviors.

RFA treatment promoted residual cancer cell proliferation via *increasing HSP70 protein*

To clarify the biological changes in residual cancer cells after RFA, cellular apoptosis was assessed following thermal treatment *in vitro*. After thermal treatment for 10 min at 37–50°C, the apoptotic rates of PANC-1 and BxPC-3 cells were both significantly increased to nearly 10%, but most cells survived (Supplemental Figure 2A). After 48 h of post-thermal treatment of PANC-1 and BxPC-3, cellular proteins were extracted and high-throughput protein mass spectrometry was applied to detect differentially expressed proteins. There were 160 differentially expressed proteins in PANC-1 cells compared to control cells and 189 differentially expressed proteins in BxPC-3 cells. Among these differentially expressed proteins, 107 overlapped (Supplemental Figure 2B), and HSP70 emerged as the protein affected the most by the treatment. Then, the expression of HSP70 was detected in the pancreatic cancer cell lines PANC-1, BxPC-3, SW1990, and MIA-PaCa-2, and the normal pancreatic ductal cells HPDE. qRT-PCR and western blot analyses showed that pancreatic cancer cell lines had higher expression than normal pancreatic ductal cells (Figure 3A and B). Among these cell lines, PANC-1 showed the highest expression of HSP70, while MIA-PaCa-2 showed the lowest. Furthermore, we found that 24, 48, and 72 h post-thermal treatment HSP70 expression was increased at both protein and mRNA levels in MIA-PaCa-2 cells (Figure 3C and D). Concomitantly, IHC staining of residual tumor tissues from orthotopic PDAC murine models showed that HSP70 levels were significantly enhanced post-RFA treatment (Figure 3E).

Then, lentiviral vectors containing the HSP70 cDNA were constructed and transfected into

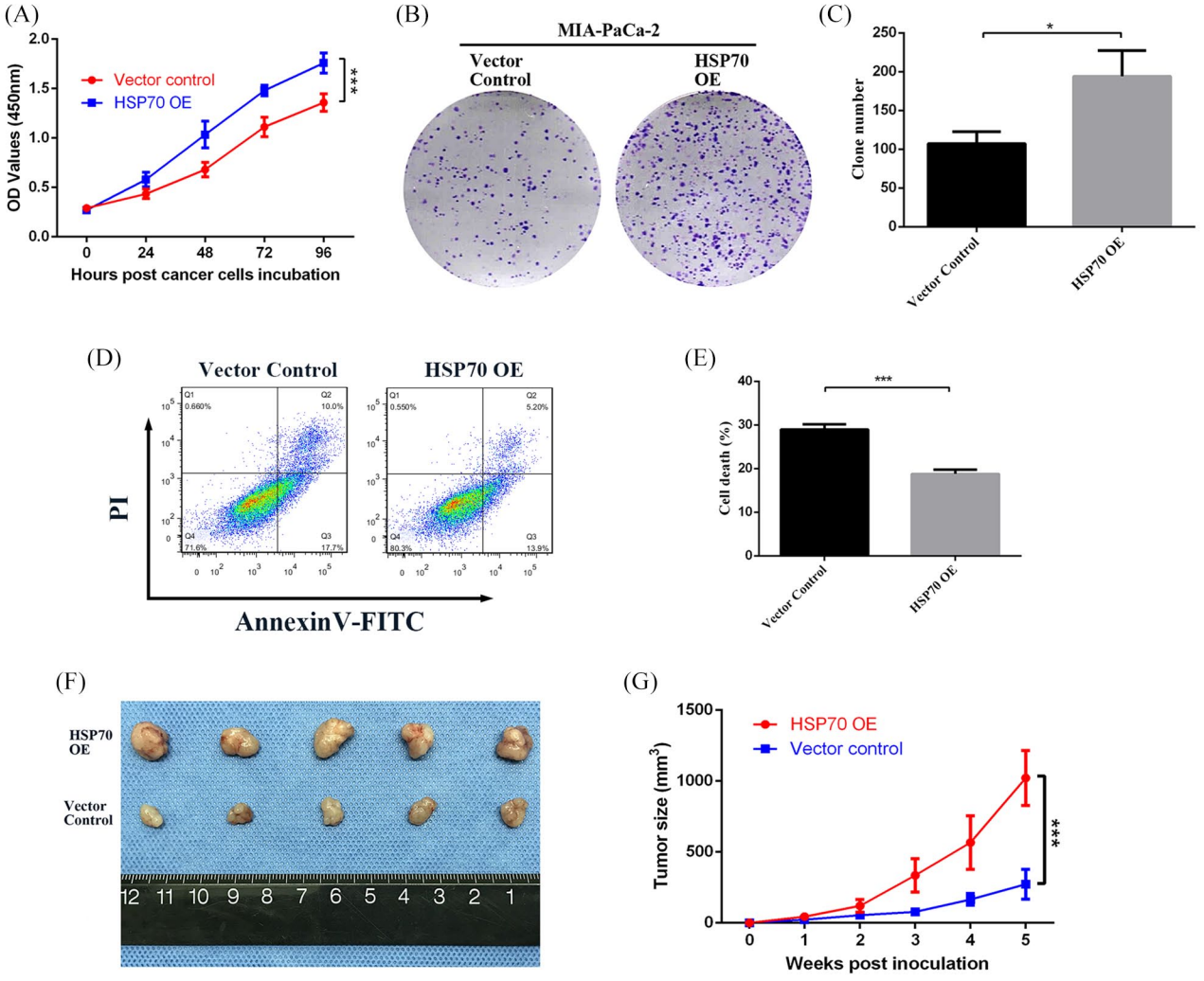

Figure 4. HSP70 promotes cell proliferation and tumor growth. (A) CCK-8 assay on 0, 24, 48, 72, and 96 h, and (B, C) colony formation assay following culture for 2 weeks showing cell proliferative ability after HSP70 overexpression in MIA-PaCa-2 cells. (D) Flow cytometry data and (E) statistical diagram showing the apoptotic rate in HSP70-overexpressing MIA-PaCa-2 and vector control cells. (F, G) Tumor volumes and growth rates of HSP70 overexpressing *versus* vector control MIA-PaCa-2 cells in nude mice models.
HSP70, heat shock protein 70.
*p-value < 0.05, **p-value < 0.01, ***p-value < 0.001.

MIA-PaCa-2 cells to overexpress (OE) HSP70, which was verified by qRT-PCR and western blot (Supplemental Figure 3A–C) as well as HSP70 knockdown (KD) of PANC-1 (Supplemental Figure 3D–F). Cell proliferation and colony formation were assessed by the CCK-8 and colony formation assays. HSP70-OE MIA-PaCa-2 cells showed a significantly enhanced proliferative rate and colony formation compared to cells transfected with vector controls (Figure 4A–C). In contrast, when HSP70 was knocked down in PANC-1 cells, their proliferative and colony formation abilities were notably decreased (Supplemental Figure 4A–C). In addition, the average apoptotic rate of HSP70-OE MIA-PaCa-2 cells assessed by flow cytometry was $18.78 \pm 0.96\%$, which was significantly lower than that of vector control cells, which was $28.97 \pm 1.17\%$ (Figure 4D and E). However, the average apoptotic rate of HSP70-KD PANC-1 cells was up to $25.32 \pm 3.89\%$ compared to $13.62 \pm 0.27\%$ of vector control cells (Supplemental Figure 4D–E).

To validate further the role of HSP70 *in vivo*, BALB/c nude mice were inoculated with HSP70-OE MIA-PaCa-2 cells, HSP70-KD PANC-1 cells or their relevant vector control cells. The tumor growth curves showed that the xenograft tumor volumes

from HSP70-OE MIA-PaCa-2 cells were significantly larger than those from vector control cells ($p < 0.001$; Figure 4F and G), and the xenografts from HSP70-KD PANC-1 were dramatically smaller than those from vector control cells ($p < 0.05$; Supplemental Figure 4F and G). Hence, HSP70 can apparently promote pancreatic cancer growth in nude mice, which indicates its critical role in tumorigenesis and progression.

HSP70 promoted PDAC progression by activating AKT–mTOR signaling pathway

The canonical pathway analysis of differentially expressed proteins identified by mass spectrometry showed the highest up-regulation for the mTOR signaling pathway (Supplemental Figure 2C). A previous publication has reported that the mTOR signaling serves as the downstream of AKT, and another HSP family member, HSP90, could significantly modulate AKT activity.[20] Thus, we hypothesized that HSP70 promoted pancreatic cancer growth *via* the AKT–mTOR signaling pathway.

Then, we assessed the impact of HSP70 on AKT–mTOR signaling by examining the expression of AKT, mTOR, p70S6K, 4EBP1, and their phosphorylated variants. The western blot results showed that the levels of phosphorylated AKT, mTOR, p70S6K, and 4EBP1 were notably increased after HSP70 overexpression, which indicated that the AKT–mTOR signaling pathway was significantly activated (Figure 5A). In contrast, AKT, mTOR, p70S6K and 4EBP1 phosphorylation were remarkably decreased when HSP70 was knocked down (Figure 5B).

To validate that HSP70 promotes pancreatic cancer cell proliferation directly by activating the mTOR signaling, the mTOR inhibitor INK-128 was utilized to reverse the mTOR-mediated proliferation induced by HSP70. The apoptotic rate of HSP70 OE cells ($12.09 \pm 0.36\%$) was lower than the $21.31 \pm 0.19\%$ of vector control cells, which was significantly reversed by adding the mTOR inhibitor ($34.81 \pm 2.72\%$, $p < 0.001$; Figure 5C and D). Similarly, the CCK-8 and colony formation assays showed that the HSP70-enhanced proliferation and colony formation abilities were significantly reversed by the mTOR inhibitor (Figure 5D–F). Concomitantly, we could observe that the HSP70-enhanced phosphorylation of mTOR downstream targets, p70S6K and 4EBP1, was completely inhibited by the mTOR inhibitor (Figure 5H). Thus, HSP70 activates mTOR signaling and promotes pancreatic cancer proliferation.

Then, an AKT inhibitor was further administered to verify that HSP70 activates mTOR signaling through AKT to promote pancreatic cancer proliferation. So, analysis of cell apoptosis by flow cytometry indicated that the apoptotic rate of HSP70 OE cells was significantly reversed by the AKT inhibitor (Figure 6A and B). In addition, the proliferation and colony formation abilities assessed by CCK-8 and colony formation assays were enhanced when HSP70 was overexpressed, which were then significantly suppressed by adding the AKT inhibitor (Figure 6C–E). Notably, the enhanced phosphorylation of AKT, mTOR, p70S6K, and 4EBP1 induced by HSP70 was inhibited by the AKT inhibitor, which confirmed that HSP70 promoted AKT–mTOR signal activation to facilitate proliferation.

RFA treatment in combination with an mTOR inhibitor in vivo *restrained PDAC growth*

Obviously, RFA treatment can enhance immune response in residual tumor tissues, but adversely promote residual cancer cell proliferation *via* activating AKT–mTOR signaling through elevation of HSP70. Thus, we proposed a combination treatment with RFA and an mTOR inhibitor to obtain a robust synergetic inhibition. Subcutaneous murine tumor models were established in immunocompetent C57BL/6 mice and the schema of RFA and INK-128 therapy is displayed in Figure 7A. At 2 weeks following treatment with the combination of RFA and the mTOR inhibitor, the average tumor volume was $951.63 \pm 250.79\,mm^2$, significantly smaller than that of the other three groups (Figure 7B and C). However, the average tumor volume following treatment with RFA alone was $1889.63 \pm 628.99\,mm^2$, the mTOR inhibitor alone $1596.88 \pm 146.27\,mm^2$ and the control treatment $2054.63 \pm 480.86\,mm^2$, which was not significantly different between these three groups. Therefore, RFA treatment in combination with an mTOR inhibitor can exert a powerful synergetic effect in tumor suppression.

Discussion

In this study, we observed the changes in immune patterns of the tumor microenvironment and the biological behaviors of residual cancer cells after RFA treatment. It is known that there are three

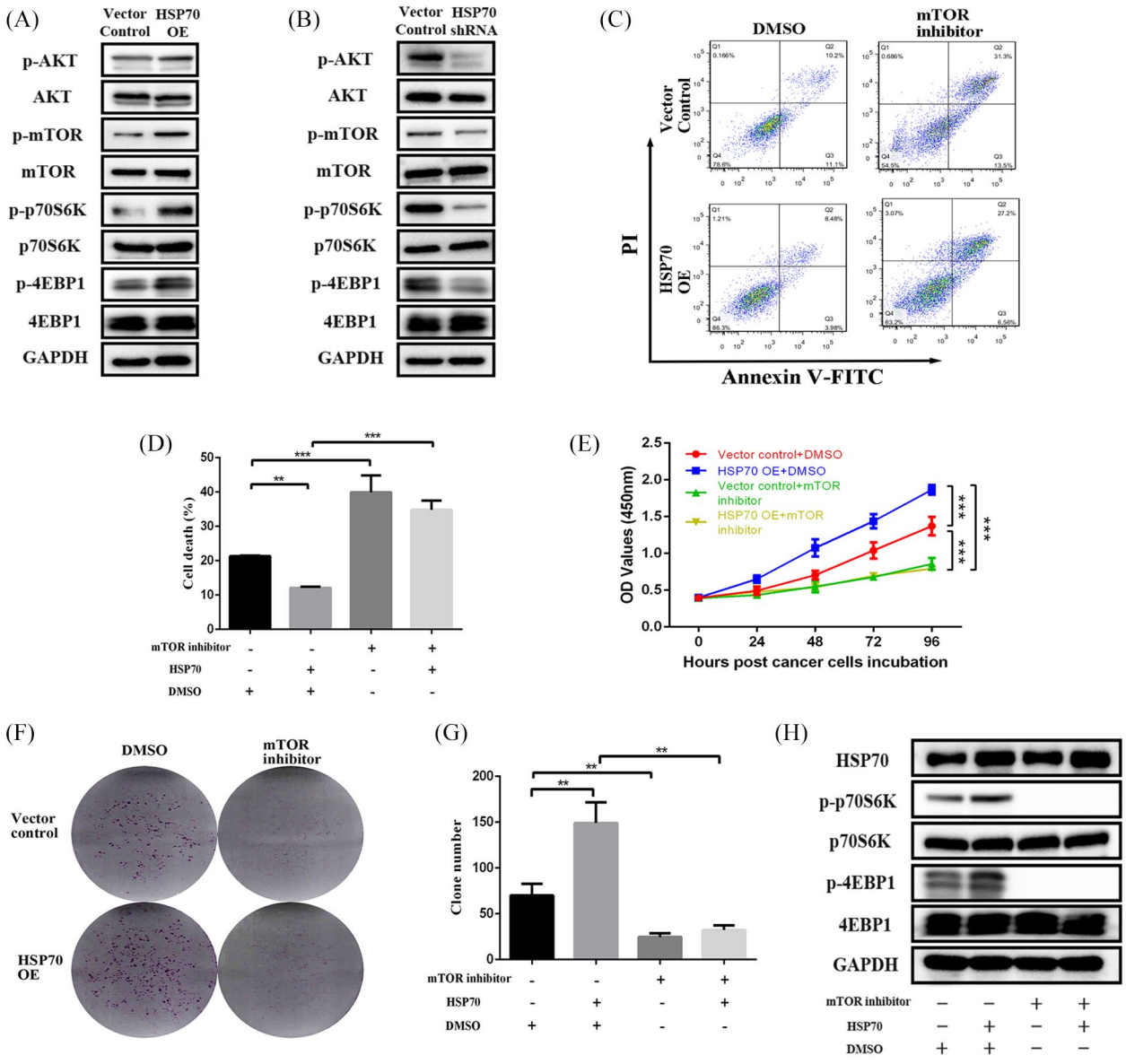

Figure 5. HSP70 promotes pancreatic cancer cell proliferation by activating the mTOR signaling pathway. Western blot analysis of the AKT–mTOR signaling pathway changes when (A) HSP70 OE in MIA-PaCa-2 cells and (B) HSP70 KD in PANC-1 cells. (C, D) Flow cytometry analysis of changes in apoptosis of the HSP70 OE MIA-PaCa-2 cells treated with 0.5 uM INK-128. (E) CCK-8 assays at 0, 24, 48, 72, 96 h, and (F, G) colony formation assays following culture for 2 weeks showing cell proliferative ability changes in HSP70 OE MIA-PaCa-2 cells treated with 0.5 uM INK-128. (H) Western blot analysis of mTOR signaling changes in HSP70 OE MIA-PaCa-2 cells treated with 0.5 uM INK-128.
HSP70, heat shock protein 70; KD, knockdown; OE, overexpression.
$^{**}p$-value < 0.01, $^{***}p$-value < 0.001.

concentric circles in the tumor tissues post-RFA treatment, the intermediate is the transition area of heat containing incomplete necrotic and apoptotic cancer cells. There, large numbers of neoantigens are exposed to recruit tumor-infiltrating immune cells and promote tumor immune response.[6] In our preclinical murine models, treatment with RFA resulted in a significant increase in tumor-infiltrating $CD8^+$ T cells and a decrease in immunosuppressive Treg cells. Furthermore, the INF-γ content of tumor tissues was relatively elevated, and TGF-β was decreased, which further indicated a decline in tumor suppression and enhancement of local immune response. Tumor-infiltrating $CD8^+$ T cells are the major effector cells to eliminate cancer cells

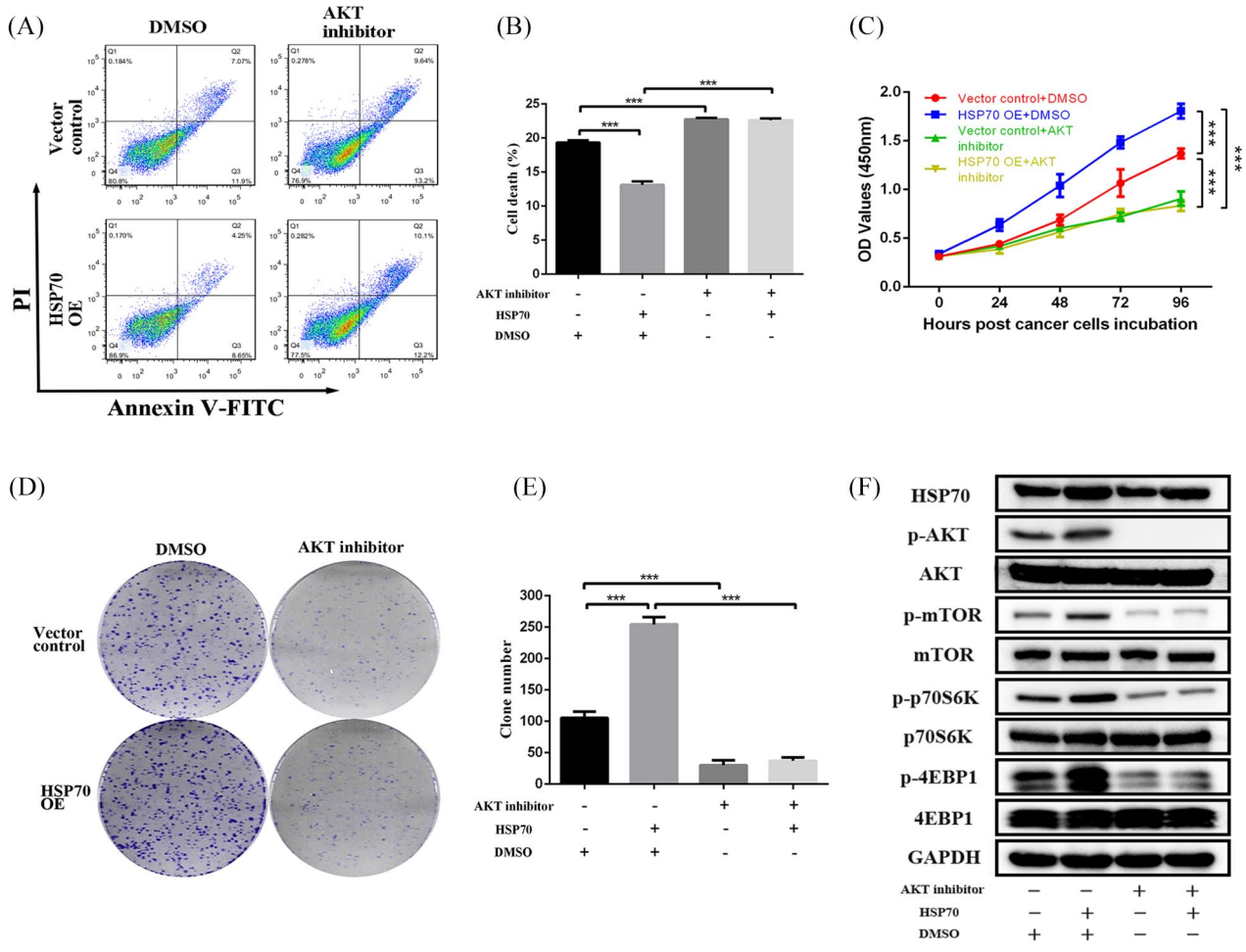

Figure 6. HSP70 activates mTOR signaling *via* AKT to promote pancreatic cancer cell proliferation. (A, B) Flow cytometry analysis of cell apoptosis changes in HSP70 OE MIA-PaCa-2 cells treated with 1 uM MK-2206. (C) CCK-8 assays at 0, 24, 48, 72, 96 h, and (D, E) colony formation assays following culture for 2 weeks showing cell proliferative ability changes in HSP70 OE MIA-PaCa-2 cells treated with 1 uM MK-2206. (F) Western blot analysis of AKT–mTOR signaling changes in HSP70 OE MIA-PaCa-2 cells treated with 1 uM MK-2206.
HSP70, heat shock protein 70; OE, overexpression.
***p-value < 0.001.

by releasing perforin, granzyme and INF-γ.[21] However, Tregs are one of the main immunosuppressive cells that suppress induction and proliferation of $CD8^+$ T cells and secrete immunosuppressive cytokines containing TGF-β and interleukin 10 (IL10) to promote cancer progression.[22–24] Zerbini *et al.*[25] have reported that cellular debris resulting from RFA treatment had the potential ability to recruit $CD8^+$ T cells and improve their specific recognition to attack cancer cells. In addition, Dromi *et al.*[26] have also reported that thermal ablation could release large amounts of tumor debris and immunogenic molecules including risk associated molecular patterns, which induce the activation and maturation of dendritic cells and $CD8^+$ T cells. A great number of studies have observed that tumor-infiltrating Tregs are significantly associated with OS of PDAC patients.[27] Thus, an increase in tumor-infiltrating $CD8^+$ T cells and a decrease in tumor-infiltrating Tregs post-RFA treatment provide a promising strategy for LAPC therapy. In addition, the decline in peripheral Tregs indicated an enhancement of systemic immune response, which may be beneficial to some tiny lesions.

However, even though RFA treatment could significantly promote tumor immune response, no actual benefit was observed in tumor growth. With *in vitro* thermal stimulation and mass spectrometry analysis, the major effector protein HSP70 was induced by RFA and found to

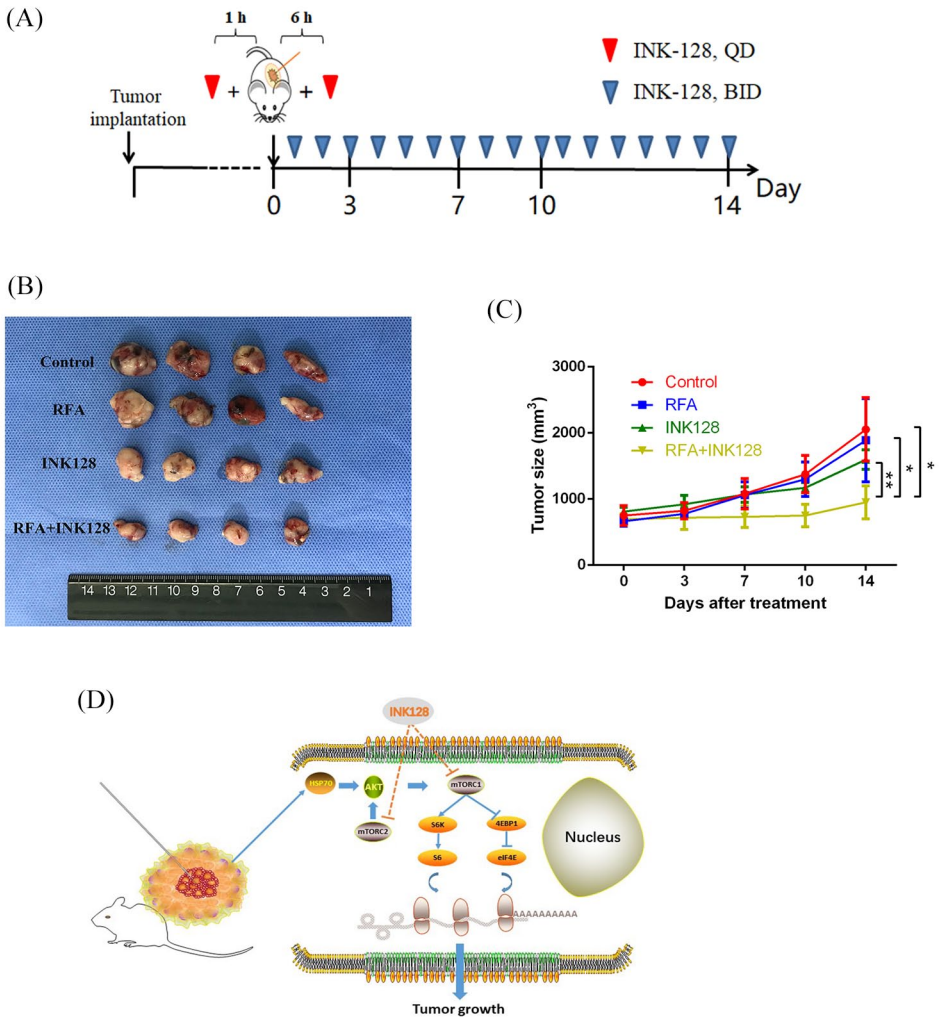

Figure 7. RFA treatment in combination with an mTOR inhibitor *in vivo* restrains PDAC growth. (A) The schema of RFA and INK-128 administration. (B, C) The tumor volumes and growth rates after treatment of RFA and INK-128 in murine PDAC models. (D) Schema showing the mechanism of the effects of RFA treatment in combination with an mTOR inhibitor.
PDAC, pancreatic ductal adenocarcinoma; RFA, radiofrequency ablation.
*p-value < 0.05, **p-value < 0.01.

promote residual cancer cell proliferation. HSP70 is a widely distributed chaperone protein, which can protect cells from thermal treatment, oxidative stress and cytotoxic drugs.[28–30] However, previous studies have revealed that the increased expression of HSP70 in breast cancer and renal cancer was strongly associated with malignant phenotypes.[31] Besides its role in the promotion of proliferation, HSP70 has been reported to be related with chemoresistance to gemcitabine, opotecan, cisplatin, adriamycin, and 5-fluorouracil.[32–34] We found that RFA treatment induced the expression of HSP70 and promoted PDAC cell proliferation *via* activating the AKT–mTOR signaling, which has been shown to regulate gene translation, cell death and proliferation.[35] The downstream effectors of mTOR pathways, 4EBP1 and p70S6K acting as two parallel pathways, independently control translation and cell survival fate.[36] Our results showed that HSP70 could promote phosphorylation of 4EBP1 and p70S6K to activate mTOR signaling. A large number of studies have reported that AKT–mTOR signaling plays a critical role in tumor progression and chemoresistance.[37–39] In this study, activation of AKT by phosphorylation was further confirmed when HSP70 was increased, which may further activate mTOR *via* TSC2 phosphorylation that subsequently stimulates Rheb, which then activates the multiprotein complex mTORC1 and

mTORC2.[40] In addition, mTOR inhibitors instead of HSP70 inhibitors were chosen to interfere with this signaling, as mTOR inhibitors could not only suppress the HSP70 induced signaling, but also several other pro-oncogenic pathways. This way, we may allow the use of minimum drug concentrations, but achieve a maximum effect. If we target HSP70 directly, it is difficult to ensure adequate doses to neutralize the HSP70, because of its induction by the environment.

Generally, RFA treatment can elevate the expression of HSP70 in residual cancer cells located in the transition area, then phosphorylate AKT to activate mTOR signaling, which promotes 4EBP1 and p70S6K phosphorylation, and finally accelerates PDAC growth (Figure 7D). Considering other regulators of mTOR signaling, such as YAP and AMPK,[41] an mTOR inhibitor was applied to block this pathway. INK-128, a new mTOR inhibitor, can inhibit both phosphorylation of 4EBP1 and p70S6K while the first generation inhibitors can only inhibit p70S6K.[42] INK-128 has been shown to be potentially efficacious in osteosarcoma, non-small cell lung cancer, B-cell acute lymphoblastic leukemia, colorectal cancer, liver cancer, and pancreatic cancer.[43–46] In addition, an additional suppression of AKT may also be observed by INK-128 treatment.[47] Thus, RFA treatment in combination with INK-128 may be a promising strategy for PDAC. In our preclinical murine PDAC models, RFA treatment combined with mTOR blockade had a synergetic effect on the suppression of tumor growth, while the single regimens showed no difference in therapeutic effects. However, further preclinical validations and clinical trials are still needed for approval of such a strategy.

There are some limitations to this study. First, we did not examine whether treatment with a higher dosage of the mTOR inhibitor combined with RFA leads to a higher efficacy. Second, we just chose the cell line (MIA-PaCa-2) with the lowest expression of HSP70 to overexpress it, and the cell line (PANC-1) with the highest expression of HSP70 to knock it down. Rescue experiments should be further performed to ascertain that the findings were due to HSP70 itself. Third, although statistical significance was reached, the number of mice included in each treatment cohort was small. Fourth, we only focused on biological changes of tumor cells induced by enhanced HSP70 that was affected the most by the RFA treatment, but ignored other potential influences from the local environment. Nevertheless, this study was the first to our knowledge to provide proof of the concept that the combination of RFA and mTOR inhibitors has therapeutic effects on pancreatic cancer in a mouse model.

In conclusion, RFA treatment in combination with mTOR signaling blockade can not only promote tumor immune response, but also restrain residual cancer cell proliferation resulting from HSP70-induced AKT–mTOR signaling activation. It is essential to understand the underlying mechanisms of changes in immune patterns and biological behaviors post-RFA treatment. Such a combination may be a promising and effective strategy for LAPC patients.

Acknowledgements

The authors thank the China Scholarship Council for supporting Dr Gao as a visiting PhD candidate at Washington University School of Medicine and Johns Hopkins University School of Medicine. They would also like to thank Editage (www.editage.com) for English language editing.

Authors' contributions

SSG, NP, LXL, JY, and XLW conceived and designed the experiments. SSG, NP, and HLY performed the experiments. SSG, NP, JHL, QDC, MJY, WHL, YC, GFZ, CYL, ZPY and LXL acquired and analyzed the data. SSG and NP wrote the manuscript. All authors read, edited and approved the final manuscript.

Conflict of interest statement

The authors declare that there is no conflict of interest.

Ethics approval

All protocols for animal use and research were reviewed and approved by the Research Ethics, Institutional Animal Care and Use Committee of Zhongshan Hospital, Fudan University (no. 2018-131).

Funding

The authors disclosed receipt of the following financial support for the research, authorship, and/or publication of this article: This work was funded by the Project of Shanghai Municipal Health Commission (no. 201940409).

Supplemental material

Supplemental material for this article is available online.

References

1. Siegel RL, Miller KD and Jemal A. Cancer statistics, 2020. *CA Cancer J Clin* 2020; 70: 7–30.
2. Ducreux M, Cuhna AS, Caramella C, *et al.* Cancer of the pancreas: ESMO clinical practice guidelines for diagnosis, treatment and follow-up. *Ann Oncol* 2015; 26 (Suppl. 5): v56–v68.
3. Gao S, Wu M, Chen Y, *et al.* Lactic dehydrogenase to albumin ratio in prediction of unresectable pancreatic cancer with intervention chemotherapy. *Future Oncol* 2018; 14: 1377–1386.
4. Liang C, Shi S, Meng Q, *et al.* Complex roles of the stroma in the intrinsic resistance to gemcitabine in pancreatic cancer: where we are and where we are going. *Exp Mol Med* 2017; 49: e406.
5. Uzunparmak B and Sahin IH. Pancreatic cancer microenvironment: a current dilemma. *Clin Transl Med* 2019; 8: 2.
6. Chu KF and Dupuy DE. Thermal ablation of tumours: biological mechanisms and advances in therapy. *Nat Rev Cancer* 2014; 14: 199–208.
7. Wissniowski TT, Hansler J, Neureiter D, *et al.* Activation of tumor-specific T lymphocytes by radio-frequency ablation of the VX2 hepatoma in rabbits. *Cancer Res* 2003; 63: 6496–6500.
8. Waitz R and Solomon SB. Can local radiofrequency ablation of tumors generate systemic immunity against metastatic disease? *Radiology* 2009; 251: 1–2.
9. Zamarron BF and Chen W. Dual roles of immune cells and their factors in cancer development and progression. *Int J Biol Sci* 2011; 7: 651–658.
10. Scopelliti F, Pea A, Conigliaro R, *et al.* Technique, safety, and feasibility of EUS-guided radiofrequency ablation in unresectable pancreatic cancer. *Surg Endosc* 2018; 32: 4022–4028.
11. Fegrachi S, Walma MS, de Vries JJJ, *et al.* Safety of radiofrequency ablation in patients with locally advanced, unresectable pancreatic cancer: a phase II study. *Eur J Surg Oncol* 2019; 45: 2166–2172.
12. Rombouts SJE, Derksen TC, Nio CY, *et al.* Computed tomography findings after radiofrequency ablation in locally advanced pancreatic cancer. *Abdom Radiol* 2018; 43: 2702–2711.
13. Hlavsa J, Prochazka V, Andrasina T, *et al.* Radiofrequency ablation in pancreatic cancer. *Rozhl Chir* 2019; 98: 441–449.
14. Matsui Y, Nakagawa A, Kamiyama Y, *et al.* Selective thermocoagulation of unresectable pancreatic cancers by using radiofrequency capacitive heating. *Pancreas* 2000; 20: 14–20.
15. Kong J, Kong J, Pan B, *et al.* Insufficient radiofrequency ablation promotes angiogenesis of residual hepatocellular carcinoma via HIF-1alpha/VEGFA. *PLoS One* 2012; 7: e37266.
16. Feng K and Ma KS. Value of radiofrequency ablation in the treatment of hepatocellular carcinoma. *World J Gastroenterol* 2014; 20: 5987–5998.
17. Wu L, Wang C, Yao X, *et al.* Application of 3.0 tesla magnetic resonance imaging for diagnosis in the orthotopic nude mouse model of pancreatic cancer. *Exp Anim* 2014; 63: 403–413.
18. Pu N, Gao S, Yin H, *et al.* Cell-intrinsic PD-1 promotes proliferation in pancreatic cancer by targeting CYR61/CTGF via the hippo pathway. *Cancer Lett* 2019; 460: 42–53.
19. Pu N, Zhao G, Yin H, *et al.* CD25 and TGF-beta blockade based on predictive integrated immune ratio inhibits tumor growth in pancreatic cancer. *J Transl Med* 2018; 16: 294.
20. Sato S, Fujita N and Tsuruo T. Modulation of Akt kinase activity by binding to Hsp90. *Proc Natl Acad Sci USA* 2000; 97: 10832–10837.
21. Rousalova I and Krepela E. Granzyme B-induced apoptosis in cancer cells and its regulation (review). *Int J Oncol* 2010; 37: 1361–1378.
22. Nishikawa H and Sakaguchi S. Regulatory T cells in cancer immunotherapy. *Curr Opin Immunol* 2014; 27: 1–7.
23. Adeegbe DO and Nishikawa H. Natural and induced T regulatory cells in cancer. *Front Immunol* 2013; 4: 190.
24. Haque S and Morris JC. Transforming growth factor-beta: a therapeutic target for cancer. *Hum Vaccin Immunother* 2017; 13: 1741–1750.
25. Zerbini A, Pilli M, Fagnoni F, *et al.* Increased immunostimulatory activity conferred to antigen-presenting cells by exposure to antigen extract from hepatocellular carcinoma after radiofrequency thermal ablation. *J Immunother* 2008; 31: 271–282.
26. Dromi SA, Walsh MP, Herby S, *et al.* Radiofrequency ablation induces antigen-presenting cell infiltration and amplification of weak tumor-induced immunity. *Radiology* 2009; 251: 58–66.

27. Liu L, Zhao G, Wu W, *et al*. Low intratumoral regulatory T cells and high peritumoral CD8(+) T cells relate to long-term survival in patients with pancreatic ductal adenocarcinoma after pancreatectomy. *Cancer Immunol Immunother* 2016; 65: 73–82.
28. Mosser DD, Caron AW, Bourget L, *et al*. Role of the human heat shock protein hsp70 in protection against stress-induced apoptosis. *Mol Cell Biol* 1997; 17: 5317–5327.
29. Calderwood SK, Khaleque MA, Sawyer DB, *et al*. Heat shock proteins in cancer: chaperones of tumorigenesis. *Trends Biochem Sci* 2006; 31: 164–172.
30. Hayashi S, Kano E, Tsuji K, *et al*. Modification of thermosensitivity and chemosensitivity induced by combined treatments with hyperthermia and adriamycin. *Int J Mol Med* 2001; 8: 417–422.
31. Elmallah MIY, Cordonnier M, Vautrot V, *et al*. Membrane-anchored heat-shock protein 70 (Hsp70) in cancer. *Cancer Lett* 2020; 469: 134–141.
32. Tang Q, Yuan Q, Li H, *et al*. miR-223/Hsp70/JNK/JUN/miR-223 feedback loop modulates the chemoresistance of osteosarcoma to cisplatin. *Biochem Biophys Res Commun* 2018; 497: 827–834.
33. Grivicich I, Regner A, Zanoni C, *et al*. Hsp70 response to 5-fluorouracil treatment in human colon cancer cell lines. *Int J Colorectal Dis* 2007; 22: 1201–1208.
34. Sluder IT, Nitika, Knighton LE, *et al*. The Hsp70 co-chaperone Ydj1/HDJ2 regulates ribonucleotide reductase activity. *PLoS Genet* 2018; 14: e1007462.
35. Laplante M and Sabatini DM. mTOR signaling in growth control and disease. *Cell* 2012; 149: 274–293.
36. Fingar DC, Salama S, Tsou C, *et al*. Mammalian cell size is controlled by mTOR and its downstream targets S6K1 and 4EBP1/eIF4E. *Genes Dev* 2002; 16: 1472–1487.
37. Yin Y, Wang X, Li T, *et al*. MicroRNA-221 promotes breast cancer resistance to adriamycin via modulation of PTEN/Akt/mTOR signaling. *Cancer Med* 2020; 9: 1544–1552.
38. Wang K, Huang W, Sang X, *et al*. Atractylenolide I inhibits colorectal cancer cell proliferation by affecting metabolism and stemness via AKT/mTOR signaling. *Phytomedicine* 2020; 68: 153191.
39. Takashima Y, Hayano A and Yamanaka R. Metabolome analysis reveals excessive glycolysis via PI3K/AKT/mTOR and RAS/MAPK signaling in methotrexate-resistant primary CNS lymphoma-derived cells. *Clin Cancer Res* 2020; 26: 2754–2766.
40. Tan AC. Targeting the PI3K/Akt/mTOR pathway in non-small cell lung cancer (NSCLC). *Thorac Cancer* 2020; 11: 511–518.
41. Xiao F, Ouyang B, Zou J, *et al*. Trim14 promotes autophagy and chemotherapy resistance of gastric cancer cells by regulating AMPK/mTOR pathway. *Drug Dev Res* 2020; 81: 544–550.
42. Li H, Li X, Liu S, *et al*. Programmed cell death-1 (PD-1) checkpoint blockade in combination with a mammalian target of rapamycin inhibitor restrains hepatocellular carcinoma growth induced by hepatoma cell-intrinsic PD-1. *Hepatology* 2017; 66: 1920–1933.
43. Li C, Cui JF, Chen MB, *et al*. The preclinical evaluation of the dual mTORC1/2 inhibitor INK-128 as a potential anti-colorectal cancer agent. *Cancer Biol Ther* 2015; 16: 34–42.
44. Jiang SJ and Wang S. Dual targeting of mTORC1 and mTORC2 by INK-128 potently inhibits human prostate cancer cell growth in vitro and in vivo. *Tumour Biol* 2015; 36: 8177–8184.
45. Jiang H and Zeng Z. Dual mTORC1/2 inhibition by INK-128 results in antitumor activity in preclinical models of osteosarcoma. *Biochem Biophys Res Commun* 2015; 468: 255–261.
46. Lou HZ, Weng XC, Pan HM, *et al*. The novel mTORC1/2 dual inhibitor INK-128 suppresses survival and proliferation of primary and transformed human pancreatic cancer cells. *Biochem Biophys Res Commun* 2014; 450: 973–978.
47. Wilson-Edell KA, Yevtushenko MA, Rothschild DE, *et al*. mTORC1/C2 and pan-HDAC inhibitors synergistically impair breast cancer growth by convergent AKT and polysome inhibiting mechanisms. *Breast Cancer Res Treat* 2014; 144: 287–298.